Coprime Array Without Holes for DOA Approximation:

Dilleep Kumar Bhadra,
College of Engineering Bhubaneswar

***Abstract*— Due to its sparse array construction, the coprime array can efficiently reduce mutual coupling, while the difference co-array (DCA) has holes that significantly reduce the amount of uniform degrees of freedom (uDOFs). By carefully building the subarrays, we propose in this letter a new coprime array structure termed hole-free coprime array (HFCA), which can provide a hole-free DCA. Additionally, in comparison to current coprime array architectures, we calculate the ideal HFCA that may generate the greatest hole-free DCA with a given number of sensors, increasing uDOFs. Furthermore, the simulations show how much better HFCA is in terms of uDOFs, spatial resolution, and direction of arrival estimation ability.**

***Index Terms*—Direction of arrival estimation, coprime array, difference co-array, uniform degree of freedom.**

I. Introduction

DIRECTION of arrival(DOA) estimation has been widely used in fields like radar, sonar and wireless communication [1][2]. The well-performed subspace-based algorithms, such as ESPRIT [3] and MUSIC [4], are proposed to extract the DOA estimates with a linear array. However, the inter-element spacing of the array is usually smaller than half wavelength and the compact arrangement of sensors will lead to heavy mutual coupling [5].

In recent years, two kinds of sparse arrays, i.e., nested array [6] and coprime array [7], have attracted great attention. Specifically, the nested array can obtain a hole-free difference co-array(DCA), but it suffers from strong mutual coupling because a dense subarray with small inter-element spacing is involved. On the contrary, the coprime array with displaced subarrays(CADiS) [8] can enlarge the minimum distance between adjacent sensors to multiple folds of the half wavelength, which is quite attractive in reducing mutual coupling. However, the holes in the DCA of CADiS considerably reduce the achievable number of uniform degrees of freedom(uDOFs) that are depended on the contiguous segments in the DCA [9]. An example of CADiS with coprime integers 3 and 8 is provided in Fig. 1. It is illustrated clearly that only 51 uDOFs can be achieved, even though the DCA of the CADiS has 137 virtual array sensors.

Recently, many works for coprime array structure are presented to partly or fully fill the holes in the DCA and enhance the available number of uDOFs. Specifically, the augmented coprime array(ACA) [7] can obtain a larger contiguous segment in DCA by doubling the subarray with fewer sensors. The thinned coprime array(TCA) was proposed in [10], by deleting redundant sensors, the TCA can offer the same number of uDOFs as ACA with fewer sensors. In [11], the extended coprime arrays, including sliding extended coprime array(SECA) and relocating extended coprime array(RECA), were proposed by manipulating the sensors of one subarray in CADiS to increase the achievable number of uDOFs. While the aforementioned coprime arrays only can partly fill the holes in the DCA, it is pointed in [12] that the complementary co-prime array(CCA) can produce a hole-free DCA by inserting a complementary subarray into the k-times extended coprime array(kECA) [12], which can considerably enhance the uDOFs. However, the CCA owns a large compact subarray that leads to strong mutual coupling.

This letter proposes a hole-free coprime array(HFCA) by carefully assembling the subarrays to eradicate the holes in the DCA of CADiS. The main contributions of this letter are summarized as follows: 1) We provide the location set of holes in the DCA of CADiS and comprehensively analyze the hole-filling process. 2) We give the closed-form expression and specific properties of HFCA and derive the optimal HFCA with a given number of sensors to obtain the maximum number of uDOFs. 3) We provide multiple simulation results to verify the superiority of HFCA in DOA estimation and resolution performance.

Notations: diag$\{\cdot\}$denotes a diagonal matrix. $\odot$and $\otimes$ stands for the Khatri-Rao product and the Kronecker product, respectively. $[a, b]$ denotes an integer set $\{a_1 | a \le a_1 \le b, a_1 \in Z\}$, and $Z = \{0, \pm 1, \pm 2, \ldots\}$. diff($T_a$, T_b) gives a set containing the differences of elements between T_a and T_b.

Fig. 1. Example of CADiS with coprime integers 3 and 8.

II. Data Model

For a coprime array with T sensors, the sensor positions can be expressed as $d_t d$, where $t \in [0, 1, \ldots, T-1]$, $d_t \in \mathrm{T}$, T is an integer set, $d = \lambda/2$ denotes the inter-element spacing, and λ denotes the wavelength. Assume K far-field uncorrelated signals with angles ϑ_k($k \in 1, 2, \ldots, K$]) impinging on the array, the array output can be expressed as

$$\boldsymbol{x}(t) = \boldsymbol{A}\boldsymbol{s}(t) + \boldsymbol{n}(t) \tag{1}$$

where $t = 1, \ldots, J$, and J denotes the total number of snapshots. $\boldsymbol{A} = [\boldsymbol{a}(\vartheta_1), \ldots, \boldsymbol{a}(\vartheta_K)]$ denotes the direction matrix, and the k-th steering vector is $\boldsymbol{a}(\vartheta_k) = [e^{-j\pi d_0 \sin\vartheta_k}, \ldots, e^{-j\pi d_{T-1} \sin\vartheta_k}]^T$. $\boldsymbol{s}(t) = [s_1(t), \ldots, s_K(t)]^T$ is the signal vector. $\boldsymbol{n}(t)$ represents the additive white Gaussian noise vector with covariance matrix $\sigma_n^2 \boldsymbol{I}_T$, where σ_n^2 stands for noise variance. The covariance matrix of $\boldsymbol{x}(t)$ is

$$\boldsymbol{R}_{xx} = E\left[\boldsymbol{x}(t)\boldsymbol{x}^H(t)\right] = \boldsymbol{A}\boldsymbol{R}_{ss}\boldsymbol{A}^H + \sigma_n^2 \boldsymbol{I}_T \tag{2}$$

where $\boldsymbol{R}_{ss} = [\boldsymbol{s}(t)\boldsymbol{s}^H(t)] = \mathrm{diag}([\sigma_1^2, \ldots, \sigma_K^2])$ stands for the source covariance matrix and σ_k^2 denotes the power of the k-th signal.

By vectorizing the covariance matrix $\boldsymbol{R}_{xx}$[13], we can obtain

$$\boldsymbol{z} = vec(\boldsymbol{R}_{xx}) = \boldsymbol{A}_v \boldsymbol{p} + \sigma_n^2 vec(\boldsymbol{I}_T) \tag{3}$$

where $\boldsymbol{p} = [\sigma_1^2, \ldots, \sigma_K^2]^T$ can be treated as the signal vector, and $\boldsymbol{A}_v = \boldsymbol{A}^* \circledS \boldsymbol{A} = [\boldsymbol{a}^*(\vartheta_1) \otimes \boldsymbol{a}(\vartheta_1), \ldots, \boldsymbol{a}^*(\vartheta_K) \otimes \boldsymbol{a}(\vartheta_K)]$ can be regarded as the equivalent direction matrix of DCA. The location set of the virtual sensors in the DCA is given by

$$\mathrm{D} = \{z \mid z = u - v;\ u, v \in \mathrm{T}\} \tag{4}$$

By extracting the equivalent received signal from the contiguous part of DCA, then the spatial smoothing algorithms can be applied [7].

III. Hole-Free Coprime Array

A. Proposed Hole-Free Coprime Array

Definition 1. (Hole-Free Coprime Array): The location set of the sensors in HFCA can be specified by T, defined by

$$\mathrm{T} = \mathrm{T}_1 \cup \mathrm{T}_2 \cup \mathrm{T}_3 \cup \mathrm{T}_4 \tag{5}$$

where T_1, T_2, T_3 and T_4 are the location sets of four subarrays

$$\begin{cases} \mathrm{T}_1 = \{nM \mid 0 \le n \le N-1\} \\ \mathrm{T}_2 = \{(N-1)M + (2M+N) + m_1 N \mid 0 \le m_1 \le L_1\} \\ \mathrm{T}_3 = \mathrm{T}_{31} \cup \mathrm{T}_{32} = \{MN - m_2 N \mid 1 \le m_2 \le [M/2\rfloor - 1\} \\ \qquad \cup \{MN - [M/2\rfloor N - M\} \\ \mathrm{T}_4 = \{L_2 + (M+N) + m_3 \mid 0 \le m_3 \le M-1\} \end{cases} \tag{6}$$

where M and N are coprime integers and $3 \le M < N$. $L_1 = T - N - M - [M/2\rfloor - 1 \ge 1$, $L_2 = M + N(T - [M/2\rfloor - N)$.

The details of hole-filling process in HFCA are provided as follows.

The subarrays with location sets T_1 and T_2 form a CADiS, and the hole positions in the DCA of CADiS are

$$\begin{cases} \mathrm{X}_1 = \{x_1 \mid x_1 = MN - \alpha M - \beta N\} \cap [1, MN - N - M] \\ \mathrm{X}_2 = \{x_2 \mid x_2 = L_2 - (MN - \alpha M - \beta N)\} \\ \mathrm{X}_3 = \{x_3 \mid x_3 = m_4 N + M\} \\ \mathrm{X}_4 = \{x_4 \mid x_4 = m_5 N\} \end{cases} \tag{7}$$

where $\alpha \in [1, N-2]$, $\beta \in [1, M-1]$, $m_4 \in [1, M]$. As the number of elements in subarray T_2 decreases, the holes with location set X_4 will appear, and when $1 \le L_1 \le M-1$, $m_5 \in [L_1 + 1, M]$, when $L_1 > M-1$, $m_5 = 0$. It is noteworthy that only the holes on the positive axis are considered due to the symmetry property of the hole positions.

For the X_1, we assume $\beta_1 \in [1, [M/2\rfloor] \in \beta$, and rewrite x_1 as [11]

$$x_1 = MN - \alpha M - \beta_1 N = MN - \beta_1 N - M - M(\alpha - 1) \tag{8}$$

where $(\alpha - 1)M \in [0, N-3]M \in \mathrm{T}_1$.

For $\beta_2 = M - \beta_1 \in [M - [M/2\rfloor, M-1] \in \beta$, we rewrite x_1 as

$$\begin{aligned} x_1 &= MN - \alpha M - \beta_2 \\ &= M(N - \alpha - 1) - (MN - \beta_1 N - M) \end{aligned} \tag{9}$$

where $(N - \alpha - 1) \in [1, N-2] \in \mathrm{T}_1$. We can conclude from (8) and (9) that the holes with location set X_1 can be filled by inserting the sensors located at $MN - \beta_1 N$ and $MN - \beta_1 N - M$. Therefore, by inserting subarray T_3 into CADiS, the holes with location set X_1 can be filled. Furthermore, we rewrite x_2 as

$$\begin{aligned} x_2 = {} & [(2M+N) + L_1 N + (N-1)M + (\alpha - 1)M] \\ & - (MN - \beta N - M) \end{aligned} \tag{10}$$

when $\alpha = 1$, $(2M+N) + L_1 N + (N-1)M \in \mathrm{T}_2$ denotes the rightmost sensor location, which implies that the holes for $\alpha = 1$ with location set X_2 can be filled. Therefore, the remaining holes start from $L_1 N + 3M + 2N$.

The set of differences of elements between T_4 and T_1 is given by

$$\mathrm{diff}(\mathrm{T}_4, \mathrm{T}_1) = \{L_1 N + MN + 2M + 2N + m_3 - nM\} \tag{11}$$

where $m_3 \in [0, M-1]$, and $n \in [0, N-1]$. It is noteworthy that diff(T_4, T_1) can be regarded as the location set of sensors

in $[L_1N + 3M + 2\ N, L_1N + MN + 3M + 2N - 1]$, and

$$L_2 < L_1N + MN + 3M + 2N - 1 \tag{12}$$

where $L_2 = L_1N + MN + M + N$. According to (12), all the holes with location set X_2 can be filled.

The set of differences of elements between T_{31} and T_{32} is given by

$$\begin{aligned}\text{diff}(T_{31}, T_{32}) &= \{MN - m_2N - (MN - \lfloor M/2 \rfloor N - M)\} \\ &= \{(\lfloor M/2 \rfloor - m_2)\ N + M\}\end{aligned} \tag{13}$$

where $(\lfloor M/2 \rfloor - m_2) \in [1, \lfloor M/2 \rfloor - 1]$.

The set of differences of elements between T_2 and T_{31} is given by

$$\begin{aligned}\text{diff}(T_2, T_{31}) &= \{M(N-1) + (2M+N) + m_1 N \\ &\quad - (MN - m_2 N)\} \\ &= \{(m_1 + m_2 + 1)\ N + M\}\end{aligned} \tag{14}$$

where $(m_1 + m_2 + 1) \in [2,\ L_1 + \lfloor M/2 \rfloor]$.

According to (13) and (14), in the case of $L_1 \geq M - \lfloor M/2 \rfloor$, $X_3 = ([1, M]N + M) \subseteq \text{diff}(T_{31}, T_{32}) \cup \text{diff}(T_2, T_{31})$, which means that the holes with location set X_3 can be filled by inserting the subarray T_3 into CADiS.

Moreover, the set of differences of elements between T_4 and T_2 is given by

$$\text{diff}(T_4, T_2) = \{(L_1 + 1 - m_1)\ N + (M + m_3)\} \tag{15}$$

where $L_1 + 1 - m_1 \in [1, L_1 + 1]$, $M + m_3 \in [M, 2M - 1]$. In the case of $N \leq 2M - 1$ and $L_1 + 2 \geq M$ $(L_1 \geq M - 2)$, $[1, L_1 + 2]N \subseteq \text{diff}(T_4, T_2)$, which means that all the holes in location set X_4 can be filled by inserting the subarray T_4 into CADiS. In the case of $N > 2M - 1$, the holes with location set X_4 can be filled by the self difference set of T_2, i.e.,

$$\text{diff}(T_2, T_2) = \{[0, m_1]\ N\} \tag{16}$$

where $m_1 \in [1, L_1]$. In the case of $L_1 \geq M$, according to (7), $m_5 = 0$, which means the holes with location set X_4 can be filled by the set of differences of elements between T_2.

The main properties of HFCA are as follows.

Property 1: HFCA defined by (6) possesses the following properties.

a) The physical array aperture of HFCA is $3M + (T + 1 - N - \lfloor M/2 \rfloor)N - 1$.

b) The M, N and T should satisfy the following condition: In the case of $N \leq 2M - 1$, $T \geq 2M + N - 1 + \lfloor M/2 \rfloor$. In the case of $N > 2M - 1$, $T \geq M + N + 1 + \lfloor M/2 \rfloor$.

c) HFCA can generate a hole-free DCA located at $[-3M - N(T + 1 - N - \lfloor M/2 \rfloor) + 1, 3M + N(T + 1 - N - \lfloor M/2 \rfloor) - 1]$, and the achievable number of uDOFs is $2(T + 1 - N - \lfloor M/2 \rfloor)N + 6M - 1$.

B. Optimal Choice of M and N for HFCA

With a given T, the maximum number of uDOFs can be obtained by calculating the optimal choices of M and N.

TABLE I
COMPARISON OF THE NUMBER OF UDOFS FOR DIFFERENT ARRAY CONFIGURATIONS

	$T = 17$		$T = 30$	
	M, N	uDOFs	M, N	uDOFs
HFCA	$M = 3, N = 8$	161	$M = 3, N = 14$	485
SECA	$M = 5, N = 8$	147	$M = 7, N = 17$	387
RECA	$M = 5, N = 8$	147	$M = 7, N = 17$	401
MCA	$M = 5, N = 8$	89	$M = 8, N = 17$	255
TCA	$M = 7, N = 8$	125	$M = 11, N = 15$	351
RECA	$k = 2, M = 5, N = 8$	89	$k = 3, M = 3, N = 14$	367
CCA	$k = 2, M = 5, N = 10$	101	$k = 4, M = 4, N = 15$	393

For a fixed T, the number of uDOFs U is

$$\begin{aligned}U &= 2(T + 1 - N - \lfloor M/2 \rfloor)N + 6M - 1 \\ &= -2\left(N - \frac{1}{2}(T + 1 - \lfloor M/2 \rfloor)\right)^2 \\ &\quad + \frac{1}{2}(T + 1 - \lfloor M/2 \rfloor)^2 + 6M - 1\end{aligned} \tag{17}$$

According to (17), the maximum value of U can be obtained with $N = \frac{1}{2}(T + 1 - \lfloor M/2 \rfloor)$.

For odd M, the optimal M can be obtained by solving the following problem:

$$\begin{aligned}\max \quad & \frac{1}{2}[T - (M-1)/2 + 1]^2 + 6M - 1 \\ = \quad & (M - (2T - 21))^2 + 96T - 440\ /8\end{aligned} \tag{18}$$

subject to M is odd, $3 \leq M < N$ and *property* 1.*b*

When $4 < 4T - 45 < T$, $12 < T < 15$. In the case of $T = 13$ and 14, the value of $M = 4T - 45 = 7$ and 11 can be obtained, respectively. According to (6), $L_1 = T - N - M - \lfloor M/2 \rfloor - 1 \geq 1$, then $N \leq 1$ and $N \leq -4$ can be obtained, which contradicts the condition of $3 \leq M < N$. As a result, for odd M, the optimal value of $M = 3$ is obtained.

For even M, the optimal M can be obtained by solving the following problem:

$$\begin{aligned}\max \quad & \frac{1}{2}(T + 1 - M/2)^2 + 6M - 1 \\ = \quad & (M - (2T - 22))^2 + 96T - 488\ /8\end{aligned} \tag{19}$$

subject to M is even, $4 \leq M < N$ and *property* 1.*b*

When $4 < 4T - 48 < T$, $13 < T < 16$. In the case of $T = 14$ and 15, the value of $M = 4T - 48 = 8$ and 12 can be obtained, respectively. According to (6), $L_1 = T - N - M - \lfloor M/2 \rfloor - 1 \geq 1$, then $N \leq 1$ and $N \leq -5$ can be obtained, which contradicts the condition of $4 \leq M < N$. As a result, for even M, the optimal value of $M = 4$ is obtained.

An example of HFCA with $M = 3$ and $N = 8$ is provided in Fig. 2, where $T_1 = \{0, 3, 6, 9, 12, 15, 18, 21\}$, $T_2 = \{35, 43, 51, 59, 67\}$, $T_3 = 13$, and $T_4 = \{78, 79, 80\}$. It is obvious that the DCA of HFCA is hole-free and is continuous in the range $[-80, 80]$ with 161 uDOFs.

Table I gives the number of uDOFs of different coprime arrays for $T = 17$ and $T = 30$, where all the coprime arrays achieve the maximum number of uDOFs. Among all the coprime arrays, the proposed HFCA obtains the largest number of uDOFs 161

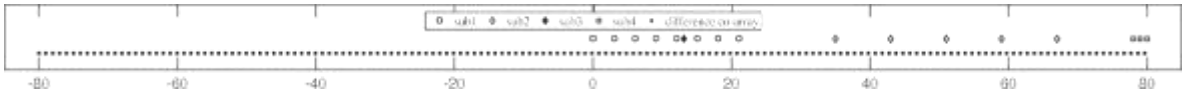

Fig. 2. Example of HFCA with $M = 3, N = 8, T = 17$.

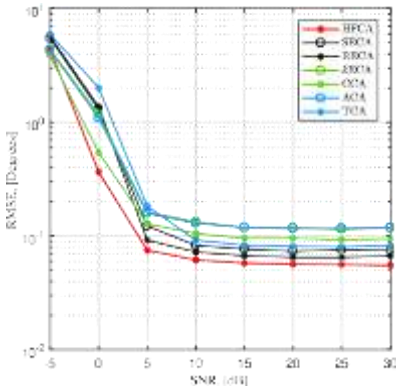

Fig. 3. RMSE comparison versus SNR.

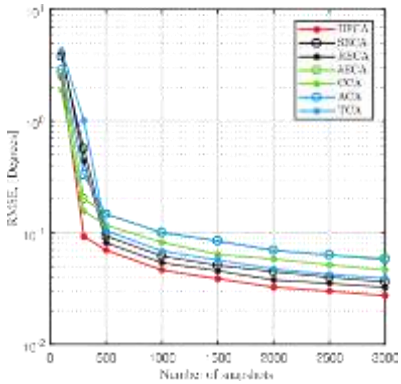

Fig. 4. RMSE comparison versus snapshot.

and 465 for $T = 17$ and $T = 30$, respectively, which exhibits the superiority of HFCA in uDOFs.

IV. Simulation Results

In this section, we only provide the simulation results to validate the performance of HFCA in DOA estimation performance due to the lack of real data at present. The simulation results exhibit the superiority of HFCA in DOA estimates. The spatial smoothing ESPRIT(SS-ESPRIT) [14] is utilized to obtain the DOA estimates in the following simulations. Besides, we use the root mean square error(RMSE) to evaluate the DOA estimation performance, which is defined by

$$\text{RMSE} = \sqrt{\frac{1}{200K}\sum_{k=1}^{K}\sum_{q=1}^{200}\left(\vartheta_k - \hat{\vartheta}_{k,q}\right)^2} \tag{20}$$

where $\hat{\vartheta}_{k,q}$ denotes the estimates of real angel ϑ_k in the q-th Monte Carlo trial.

Assume there are $K = 24$ signals impinging on the coprime arrays with $\vartheta_k = -65 + 130(k-1)/23, k \in [1, 24]$. The number of sensors for all arrays is $T = 17$, and the specifications of coprime arrays are given by Table I. The RMSE results versus the signal-to-noise ratio(SNR) are shown in Fig. 3. The snapshot is set to $J = 500$, and the SNR varies from− 5 dB to 30 dB. It is shown obviously that HFCA outperforms the other coprime arrays in DOA estimates, because it can obtain the largest contiguous segments in the DCA. In particular, although CCA can also provide a hole-free DCA, it provides less number of uDOFs than HFCA. Moreover, the ACA and kECA possess similar DOA estimation performance because of the same length of contiguous segments in DCA. The RMSE results versus the number of snapshot is shown in Fig. 4, where SNR=5 dB. It is illustrated clearly that the proposed HFCA can also achieve the best performance compared with the other coprime arrays.

In addition, we study the resolution ability of the coprime arrays with $T = 17$ sensors, where SNR = 10 dB, $J = 500$ and

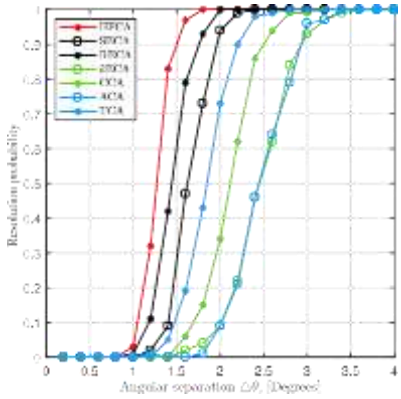

Fig. 5. Resolution probability versus angular separation.

the specifications of coprime arrays are given by Table I. Assume $K = 24$ sources impinging on the array with angles $\vartheta_k' = -65 + 130(k-1)/11, k \in [1, 12]$ and $\vartheta_k'' = \vartheta_k' + \circ\vartheta$, $\circ\vartheta$ denotes the angular separation. The 24 sources can be recognized if $|\hat{\vartheta}_k' - \vartheta_k'|$ and $|\hat{\vartheta}_k'' - \vartheta_k''|$ are smaller than $|\vartheta_k' - \vartheta_k''|/2$, where $\hat{\vartheta}_k'$ and $\hat{\vartheta}_k''$ are the DOA estimates. Fig. 5 gives the results of the resolution probability versus angular separation $\circ\vartheta$. It can be seen that HFCA can successfully recognize all the targets when $\circ\vartheta \geq 1.75^\circ$, which outperforms the other coprime arrays due to the elongated contiguous segments in the DCA.

V. Conclusion

This letter proposes the use of a new coprime array called HFCA. Through meticulous subarray assembly, the suggested HFCA can completely cover all of the holes in the CADiS DCA, yielding a DCA devoid of holes. Moreover, we derive the ideal HFCA that may achieve the largest number of uDOFs for a fixed number of sensors. Finally, simulations demonstrate the advantages of HFCA over alternative coprime arrays in terms of uDOFs, DOA estimates, and spatial resolution.

REFERENCES

[1] Li Cong and Weihua Zhuang, "Hybrid TDOA/AOA mobile user location for wideband CDMA cellular systems," *IEEE Trans. Wireless Commun.*, vol. 1, no. 3, pp. 439–447, Jul. 2002.

[2] J. Shi, G. Hu, X. Zhang, F. Sun, and H. Zhou, "Sparsity-based two-dimensional DOA estimation for coprime array: From sum-difference coarray viewpoint," *IEEE Trans. Signal Process.*, vol. 65, no. 21, pp. 5591–5604, Nov. 2017.

[3] R. Schmidt, "Multiple emitter location and signal parameter estimation," *IEEE Trans. Antennas Propag.*, vol. AE-34, no. 3, pp. 276–280, Mar. 1986.

[4] R. Roy and T. Kailath, "ESPRIT-estimation of signal parameters via rotational invariance techniques," *IEEE Trans. Acoust., Speech, Signal Process.*, vol. 37, no. 7, pp. 984–995, Jul. 1989.

[5] K. M. Pasala and E. M. Friel, "Mutual coupling effects and their reduction in wideband direction of arrival estimation," *IEEE Trans. Aerosp. Electron. Syst.*, vol. 30, no. 4, pp. 1116–1122, Oct. 1994.

[6] P. Pal and P. P. Vaidyanathan, "Nested arrays: A novel approach to array processing with enhanced degrees of freedom," *IEEE Trans. Signal Process.*, vol. 58, no. 8, pp. 4167–4181, Aug. 2010.

[7] P. P. Vaidyanathan and P. Pal, "Sparse sensing with co-prime samplers and arrays," *IEEE Trans. Signal Process.*, vol. 59, no. 2, pp. 573–586, Feb. 2011.

[8] S. Qin, Y. D. Zhang, and M. G. Amin, "Generalized coprime array configurations for direction-of-arrival estimation," *IEEE Trans. Signal Process.*, vol. 63, no. 6, pp. 1377–1390, Mar. 2015.

[9] C. Liu and P. P. Vaidyanathan, "Super nested arrays: Linear sparse arrays with reduced mutual coupling–Part I: Fundamentals," *IEEE Trans. Signal Process.*, vol. 64, no. 15, pp. 3997–4012, 2016.

[10] A. Raza, W. Liu, and Q. Shen, "Thinned coprime array for second-order difference co-array generation with reduced mutual coupling," *IEEE Trans. Signal Process.*, vol. 67, no. 8, pp. 2052–2065, Apr. 2019.

[11] W. Zheng, X. Zhang, Y. Wang, M. Zhou, and Q. Wu, "Extended coprime array configuration generating large-scale antenna co-array in massive MIMO system," *IEEE Trans. Veh. Technol.*, vol. 68, no. 8, pp. 7841–7853, Aug. 2019.

[12] X. Wang and X. Wang, "Hole identification and filling in *k*-times extended co-prime arrays for highly efficient DOA estimation," *IEEE Trans. Signal Process.*, vol. 67, no. 10, pp. 2693–2706, Oct. 2019.

[13] W. Ma, T. Hsieh, and C. Chi, "DOA estimation of quasi-stationary signals with less sensors than sources and unknown spatial noise covariance: A khatri–Rao subspace approach," *IEEE Trans. Signal Process.*, vol. 58, no. 4, pp. 2168–2180, Apr. 2010.

[14] J. Liu, Y. Zhang, Y. Lu, S. Ren, and S. Cao, "Augmented nested arrays with enhanced DOF and reduced mutual coupling," *IEEE Trans. Signal Process.*, vol. 65, no. 21, pp. 5549–5563, Nov. 2017.